Journal of Catalysis **182,** 339–348 (1999)
Article ID jcat.1998.2326, available online at http://www.idealibrary.com on IDEAL®

Zeolite-Supported Ni and Mo Catalysts for Hydrotreatments

I. Catalytic Activity and Spectroscopy

Dien Li,*,†,[1] A. Nishijima,* and D. E. Morris‡

*Department of Surface Chemistry, National Institute of Materials and Chemical Research, Tsukuba, Ibaraki 305, Japan; and †Earth and Environment Sciences Division and ‡Chemical Sciences and Technology Division, Los Alamos National Laboratory, Los Alamos, New Mexico 87545

Received June 24, 1998; revised November 5, 1998; accepted November 12, 1998

The catalytic hydrodesulfurization (HDS) of dibenzothiophene (DBT) and hydrocracking (HC) of decalin, tetralin, and diphenylmethan (DMP) over Ni–Mo sulfide catalysts supported on ultrastable Y-type (USY) zeolite have been studied. The catalysts are characterized using NH_3 temperature-programmed desorption (TPD), X-ray photoelectron spectroscopy (XPS), UV–vis–NIR diffuse reflectance spectroscopy (DRS), and Na and Al *K*-edge X-ray absorption near-edge structure (XANES). Ni–Mo sulfide catalyst supported on USY zeolite has an unusually high catalytic activity for the hydrotreating reactions of the model compounds compared with other zeolites and their supported catalysts. NH_3 TPD shows the presence of a strong acid site at about 430°C in USY zeolite and its supported Ni–Mo catalyst, which is dominantly characterized by Brønsted acidity. The surface concentrations of Ni and Mo in both calcined and sulfided Ni–Mo/USY zeolite catalysts are very low, indicating that the Ni and Mo phases are present in the crystal structure of USY zeolite. The diffuse reflectance spectra of calcined Ni–Mo/USY catalyst show that Mo is dominantly four-coordinate with oxygen and Ni is six-coordinate, consistent with the Ni and Mo species being present in the crystal structure of USY zeolite. Al *K*-edge XANES spectra of calcined Ni–Mo/USY catalyst also indicate the presence of extra-framework Al, and the content of the extra-framework Al is much higher in Ni–Mo/USY than in Ni–Mo/NaY catalyst. However, there is no evidence that the extra-framework Al contributes to the acidity and the increased catalytic activity. Thus, the high catalytic HDS and HC activities of Ni–Mo/USY compared with other zeolites and their supported Ni–Mo catalysts are attributed to the synergistic effect between the strong Brønsted acid sites and the Ni and Mo sulfide phases in the sodalite cage and/or supercage of USY zeolite.

Key Words: **zeolite-supported Ni–Mo catalysts; hydrocracking; hydrodesulfurization; NH_3 temperature-programmed desorption; X-ray photoelectron spectroscopy; diffuse reflectance spectroscopy; Na and Al *K*-edge X-ray absorption near-edge structure.**

[1] To whom correspondence should be addressed at EES-1, MS D469, Los Alamos National Laboratory, Los Alamos, NM 87545. Fax: (505) 665–3285. E-mail: dienli@lanl.gov.

INTRODUCTION

The industrial hydrotreatment of petroleum and coal liquefaction is commonly achieved with γ-Al_2O_3 supported Mo and W sulfide catalysts promoted by Co or Ni. The chemistry and structure of these catalysts, particularly Co–Mo/γ-Al_2O_3 catalyst, have been extensively investigated (1). Although alumina-supported transition-metal sulfide catalysts have high hydrogenation activity, their hydrocracking activity is relatively poor. Modern hydrocracking catalysts often are the Ni–Mo or Ni–W sulfide phases supported on zeolites (2), to achieve both high activity and flexible selectivity. In fact, these sorts of catalysts are bifunctional because transition-metal sulfides such as pure or supported Ni–Mo–S phase are effective hydrogenation catalysts, while zeolites are acidic catalysts and have good hydrocracking capability. Thus, transition-metal sulfide catalysts supported on zeolites are promising for deep hydrodesulfurization catalysis to produce clean-burning fuels (3).

Despite the extensive use of zeolites in catalysis, there has been relatively little research work on their applications in hydrotreating processes until recently. For Ni(Co)–Mo sulfide catalysts supported on zeolites, their catalytic activities have been examined for hydrocracking (HC) of *n*-heptane (4–6), alkanes (7), and *n*-decane (8, 9); hydrodesulfurization (HDS) of thiophene (10–15), ethylbenzene (16, 17), benzothiophene (18), and gas oil (19); and hydrogenation of benzene (20–22). The synergistic effects between Ni (Co) and Mo and between metal loading and acidity of zeolite have been observed for HDS activity of thiophene (10, 11) and ethylbenzene (16, 17), HC of *n*-heptane (4, 5) and hydrogenation of benzene (20–22). The synergistic effect occurs at a Ni/(Ni + Mo) ratio of about 0.4–0.5, and may be related to the formation of Ni–Mo–S phases within the structure of zeolite. Leglise *et al.* (20–22) showed using TEM that all of the Ni species and more than half of the Mo species were found in HY zeolite cavities, and MoO_3

0021-9517/99 $30.00

was also observed outside the zeolite grain; the sulfidation transforms the outside MoO_3 into MoS_2, and evicts about 50% of Ni to form a Ni–Mo–S phase in zeolite mesopores; the Ni–Mo sulfide in the zeolite is highly dispersed and responsible for the high hydrogenation activity of benzene that is comparable to that of conventional Ni–Mo/Al_2O_3 catalysts. However, Welters *et al.* (23) argued that the very small nickel and molybdenum sulfide clusters located in the zeolite supercages strongly contribute to the thiophene HDS activity and that no promoter effect has been observed in the hydrocracking of *n*-decane over Ni–Mo/zeolite Y (8). Recently, Okamoto and Katsuyama (14, 15) prepared highly dispersed Co–Mo binary sulfide clusters encapsulated in NaY zeolite cavities using $Mo(CO)_6$ and $Co(CO)_3NO$ as precursors. They showed that the HDS of thiophene takes place on the Co sites of the Co–Mo binary sulfide clusters and the Co–S–Mo bonding is responsible for the synergistic effect. Tatsumi *et al.* (18) prepared zeolite-supported Ni–Mo sulfide catalyst by ion-exchanging zeolite with Ni–Mo bimetallic sulfide cluster $[Mo_3NiS_4Cl(H_2O)_9]^{3+}$. They found that Ni–Mo/mordenite zeolite has higher activity for the HDS of benzothiophene than either sodium Y-type (NaY) zeolite or USY zeolite-supported Ni–Mo sulfide catalysts.

Thus, there is still some controversy regarding the structure, dispersion, and chemical speciation of Ni and Mo species in Ni–Mo/zeolite catalysts, as well as the mechanism of catalysis for hydrotreating reactions. In the present work, to develop new-generation catalysts for the deep HDS of petroleum and coal liquefactions, newly developed USY zeolite was used as the support to prepare Ni and Mo sulfide catalysts using conventional ion-exchange techniques. The HC reactions of tetralin, diphenylmethan (DPM), and decalin and the HDS of dibenzothiophene (DBT) have been carried out to evaluate catalytic activity. We have used NH_3 temperature-programmed desorption (TPD) to study the acid structures in both zeolite and its supported Ni–Mo catalyst; X-ray photoelectron spectroscopy (XPS) and UV–vis–NIR diffuse reflectance spectroscopy (DRS) to investigate the chemical states and structure of Ni and Mo in zeolite-supported catalysts; and Na and Al *K*-edge X-ray absorption near-edge structure (XANES) to study the change in the content and structure of Na and Al in the catalyst preparation. The relationship of the chemical states and structure of active metal phases to the hydrotreating catalytic activities is discussed. For comparison, Ni and Mo sulfide catalysts supported on NaY zeolite, mordenite, and ZSM-5 have also been studied.

EXPERIMENTAL

Catalyst Preparation

NaY zeolite, USY zeolite, and ZSM-5 were provided by Catalysts & Chemicals Industry Ltd., Japan, and H-mordenite was obtained from Tosoh, Japan. NaY zeolite was ion-exchanged with $(NH_4)_2SO_4$ solution to prepare the NH_4 form of zeolite, which was calcined at 550°C for 1 h to obtain HY zeolite. The HY zeolite was steamed at 700°C for 3 h for dealumination, and then washed using H_2SO_4 (pH 2.7) to prepare the USY zeolite. The chemical composition and BET surface area of NaY and USY zeolites are given in Table 1. Ni and Mo sulfide catalysts supported on the zeolites were prepared by conventional ion exchange of $(NH_4)_6Mo_7O_{24} \cdot 4H_2O$ and $Ni(NO_3)_2 \cdot 6H_2O$ aqueous solutions at about 60°C for 2 h. The loadings of NiO and MoO_3 were kept constant at 2 and 8 wt%, respectively, with a molar NiO/MoO_3 ratio of about 0.48. After ion exchange, the aqueous solution was evaporated at about 80°C; the Ni–Mo/zeolite slurries were dried at 200°C for 2 h in a rotary kiln and calcined at 550°C for 3 h in air. Thereafter, the catalysts were sulfided at 400°C for 2 h under a stream of H_2–H_2S mixture (the volume percentage of H_2S in the mixture was 5.04%) before the catalytic activity tests.

TABLE 1

Chemical Composition and Surface Area of Zeolites

Zeolite	SiO_2/Al_2O_3 molar ratio	Na_2O (wt%)	BET surface area (m^2/g)
NaY	4.7	10.86	763
USY	8.1	0.31	759
H-mordenite	14.7	0.39	524
ZSM-5	166.4	0.03	408

Catalytic Activity

DBT was dissolved in decalin to make the feedstock solution for the HDS of DBT that contains 1 wt% of sulfur (if not otherwise specified). The hydrotreating catalytic reactions of these model compounds were carried out using a batch microreactor, and the reaction conditions are summarized in Table 2. Three-tenths gram of sulfided zeolite-supported Ni–Mo catalyst and 10 ml feedstock solution were loaded into the reactor. The reactor was tightly closed and filled with H_2 gas whose pressure in the reactor was set at 6.92 MPa. After 1 h reaction in a high-temperature furnace, the reactor was opened and the reactant solution was

TABLE 2

Summary of Catalytic Reaction Conditions

Reaction	Reactant	Temperature (°C)	Time (h)	Pressure (MPa)	Catalyst weight (g)
HDS	DBT	340	1	6.92	0.3
HC	Decalin	340	1	6.92	0.3
HC	Tetralin	375	1	6.92	0.3
HC	DPM	375	1	6.92	0.3

transferred into a vial for gas chromatography (GC) analysis, so that some gas-phase products were not detected, and the selectivity was not calculated. For all catalytic reactions, the conversion in percentage were calculated based on the integrated areas of related target molecules in the GCs of feedstocks and the solution after reactions. The conversion rates in mol/gs were further calculated based on the percentage conversion, weight of catalysts (0.3 g), and reaction time (1 h).

Catalyst Characterization

NH_3 TPD measurements were carried out using a thermal analyzer DT-30 apparatus (Shimadzu). About 0.3 g catalyst sample charged into a glass tube was heated under He atmosphere at the rate of 30°C/min from room temperature to 500°C and kept at 500°C for another hour. The NH_3 adsorption was carried out at 150°C for 1 h and then the sample was flushed with He for another hour. Thereafter, the sample was heated again from 150 to 600°C at the rate of 10°C/min under He atmosphere for the desorption of NH_3. The NH_3 TPD profiles were decomposed by fitting and the densities of major acid sites were estimated by the integrated areas.

X-ray photoelectron spectra of the calcined catalysts were collected at a chamber pressure of $\sim 10^{-9}$ Torr (1 Torr $= 133 \times 10^{-4}$ MPa) using a Phi-5500 ESCA spectrometer (Perkin–Elmer). The monochromatized Al$K\alpha$ ($h\nu = 1486.7$ eV) was used as the exciting source. The X-ray photoelectron spectra were calibrated based on the C 1*s* binding energy of 284.6 eV. The Mo 3*d*, Ni 2*p*, and S 2*p* lines were deconvoluted by fitting. The deconvolution of the Mo 3*d* envelope was based on several constraints to give physical significance to the peaks obtained: (i) the spin–orbit splitting of the Mo 3*d* peak is 3.15 eV; (ii) the Mo $3d_{5/2}$/Mo $3d_{3/2}$ area ratio was kept constant at the theoretical value of 1.5; (iii) the full width at half-maximum (FWHM) of the Mo $3d_{5/2}$ and Mo $3d_{3/2}$ peaks of the Mo^{5+} and Mo^{6+} oxidation states were kept equal to the corresponding ones of the Mo^{4+} species (24). The atomic concentration ratios on the surface of catalysts were calculated using $n_A/n_B = I_A S_B/I_B S_A$, where n_i is the number of atoms of species i ($i =$ A or B), I_i is the integrated intensity of species i, and S_i is the sensitivity factor given by XPS measurements. The sensitivity factor depends mainly on the photoionization cross section σ_i, but also on the effects of exciting X-ray energy, takeoff angle of measurements, detector efficiency, and kinetic energy. The formula used to calculate the atomic concentration is similar to the Kerkhof–Moulijn model (25).

The UV–vis–NIR diffuse reflectance spectra of calcined zeolite-supported Ni–Mo catalysts were measured using a Lambda-19 spectrometer (Perkin–Elmer) equipped with a lab sphere model RSA-PE-19 reflectance spectroscopy attachment. The spectra were recorded over the range 200–2500 nm and at room temperature, with a spectral slit width of 4 mm. A quartz window was used in the DRS measurements, which showed absorption peaks at about 1385 and 2215 nm.

Na and Al *K*-edge XANES spectra of Y zeolites and their supported Ni–Mo catalysts were measured using the BL-7A beamline at UVSOR in the Institute for Molecular Sciences, Japan. The beamline used beryl (0001) and quartz (1010) as the monochromator crystals, respectively, for Na and Al *K*-edge XANES measurements. The storage ring was operated at an energy of 750 MeV and a current of 80–190 mA. The samples were ground into fine powder and put on the first photocathode made of the electron multiplier. Na and Al *K*-edge XANES spectra were collected using total electron yield mode, and calibrated by Na *K*-edge of NaCl at 1076.5 eV and by Al *K*-edge of Al foil at 1560.0 eV, respectively. The data point interval was 0.25 eV in the near-edge region. A linear background was removed from each spectrum.

RESULTS

Catalytic Activities

Figure 1 shows the catalytic HDS activity of DBT and HC activities of decalin, tetralin, and DPM over Ni–Mo sulfide catalysts supported on NaY zeolite, USY zeolite, mordenite, and ZSM-5. Although the HC activity of tetralin over mordenite is relatively high, the catalytic HDS and HC activities of these model compounds over mordenite and ZSM-5 zeolites and over their supported Ni–Mo sulfide catalysts are very low. The reason why mordenite-supported Ni–Mo catalyst has very low HC and HDS activities is not entirely understood by current experimental data. The catalytic activities of these model reactions over NaY zeolite and its supported Ni–Mo sulfide catalysts are also quite low, although Ni–Mo/NaY zeolite has some HDS activity. However, USY zeolite has a relatively higher activity for all these reactions compared with NaY zeolite, particularly for HC of DPM. It is most interesting that USY-supported Ni–Mo sulfide catalyst has very high activities for the HDS of DBT and the HC of decalin, tetralin, and DMP. Under the reaction conditions employed here (see Table 2), the HC activities of Ni–Mo/USY zeolite are much higher than those of conventional Ni–Mo/Al_2O_3 catalysts (26), and its HDS activity of DBT is higher than that of the Ni–Mo/Al_2O_3 catalysts (25).

Figure 2 shows variations in the HC activity of decalin and the HDS activity of DBT over USY zeolite and its supported Ni–Mo sulfide catalyst as a function of the content (wt%) of sulfur in the decalin solution containing DBT. Both HC of decalin and HDS of DBT are much higher for Ni–Mo/USY than those for USY zeolite itself. The HC conversion rate of decalin slightly decreases with increasing content of sulfur in the feedstock solution, indicating that sulfur may slightly poison the HC reaction of decalin.

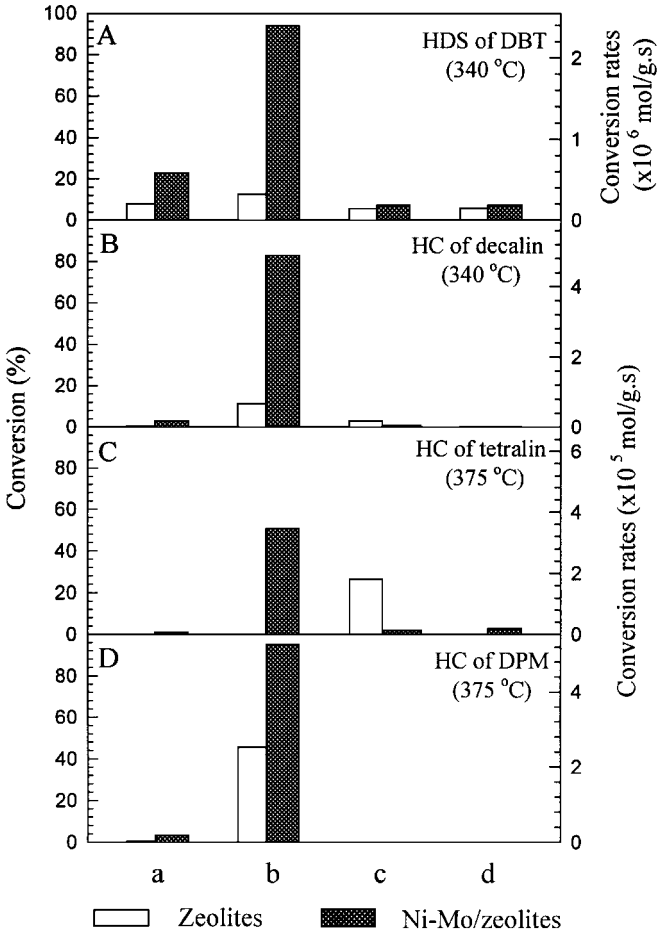

FIG. 1. Catalytic HDS activity of DBT (A) and HC activities of decalin (B), tetralin (C), and DMP (D) over zeolites (blank bars) and their supported Ni–Mo sulfide catalysts (filled bar). (a) NaY zeolite. (b) USY zeolite. (c) H-mordenite. (d) ZSM-5.

The HDS conversion rate of DBT over USY zeolite and sulfided Ni–Mo/USY catalyst shows a trend of marked increase with decreasing content of sulfur in the feedstock solution, even though this trend is not significant for sulfided Ni–Mo/USY, because the reaction conditions are too severe and its activity is too high. This result indicates that the sulfided Ni–Mo/USY catalyst is more effective for the HDS of the lower-sulfur-content feedstock, and may be used as a deep HDS catalyst.

Acid Structure of Zeolite-Supported Ni–Mo Catalysts

Figure 3 shows the NH_3 TPD profiles of zeolites and calcined Ni–Mo/zeolite catalysts. The NH_3 TPD profiles are decomposed by fitting, and the acidity densities of two major acid sites I and II estimated by the integrated areas are listed in Table 3. The loadings of Ni and Mo into zeolites do not significantly change the structure of surface acid sites, even though the total acidities of Ni–Mo/ZSM-5 and Ni–Mo/mordenite improved markedly with metal loading. The NH_3 TPD spectrum of ZSM-5 and its supported Ni–Mo catalyst shows a low-temperature peak at about 230°C (site I) and a high-temperature peak at about 410°C (site II), although the previous work suggested that the TPD spectrum of ammonium-exchanged ZSM-5 shows a single

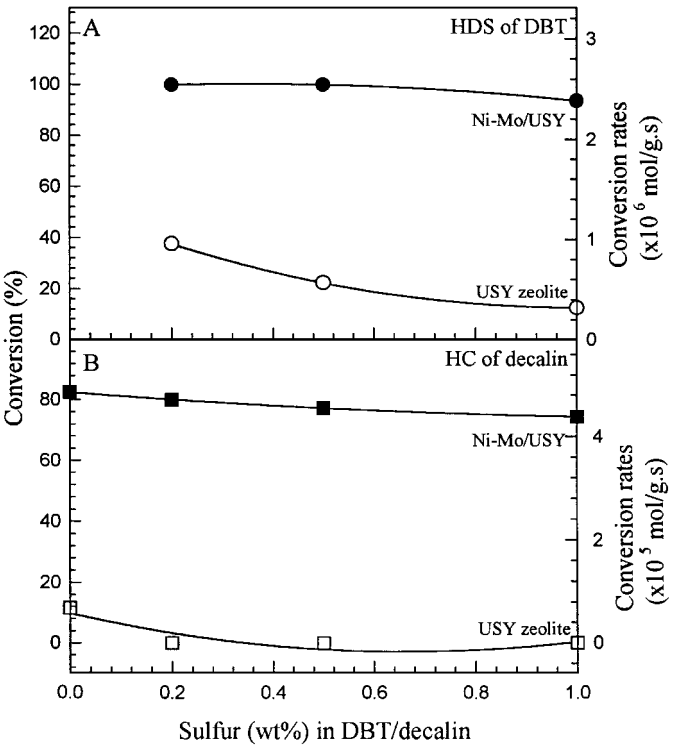

FIG. 2. Variations of the HDS activity of DBT and the HC activity of decalin over sulfided Ni–Mo/USY zeolite at 340°C with the content of sulfur in the feedstock solution.

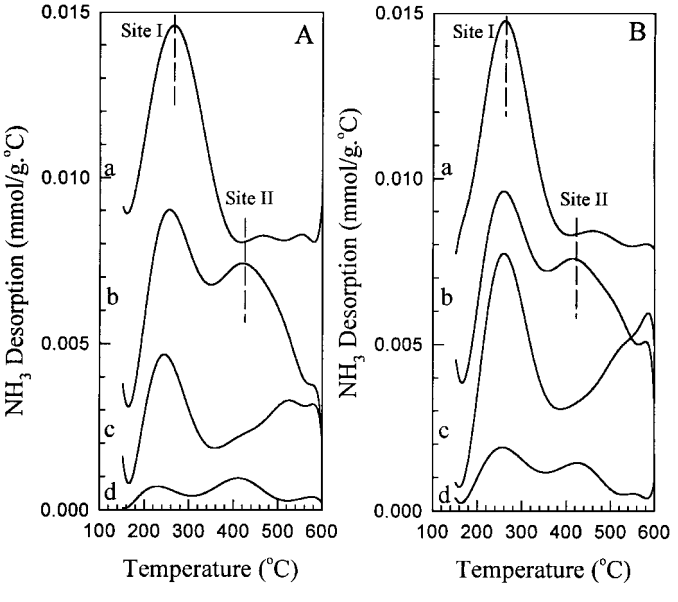

FIG. 3. NH_3 TPD profiles of zeolites (A) and their supported Ni–Mo catalysts (B). (a) NaY zeolite (b) USY zeolite (c) H-mordenite (d) ZSM-5.

TABLE 3

Acidity Density of Two Major Acid Sites of Zeolites and Their Supported Ni–Mo Catalysts

Sample	Acid site I		Acid site II	
	Strength (°C)	Density (mmol/g)	Strength (°C)	Density (mmol/g)
NaY zeolite	267	0.9260	472	0.0134
USY zeolite	259	0.9235	406	0.6885
Mordenite	251	0.5723	414	0.2982
ZSM-5	234	0.0720	407	0.1468
Ni–Mo/NaY	264	0.9679	470	0.0786
Ni–Mo/USY	263	0.8904	419	0.6474
Ni–Mo/mordenite	262	0.9128	412	0.4988
Ni–Mo/ZSM-5	259	0.2351	407	0.2197

desorption band at 400°C (27). The high-temperature peak is related to protonic acidity, while the low-temperature peak is probably due to ammonia coordinated to aluminum species. The total number of these acid sites in ZSM-5 and its supported catalyst is relatively small. In NaY zeolite and mordenite, there is a dominant acid site at about 250°C that may be characterized as a Lewis acid site. However, the most distinctive feature is that USY zeolite and its supported Ni–Mo catalyst have another strong acid site at about 410°C (site II). The 410°C acid site in USY zeolite may be characterized as a Brønsted acid feature (28).

Surface Concentrations of Ni and Mo Species

The Mo 3*d* X-ray photoelectron spectra of calcined and sulfided Ni–Mo catalysts are shown in Fig. 4. The Mo 3*d* X-ray photoelectron spectra of the calcined catalysts are similar, but different in the relative intensity, and can be decomposed into a doublet by fitting (24). The two prominent peaks are assigned to the spin–orbit split Mo^{6+} $3d_{5/2}$ (BE ≅ 232.6 eV) and Mo^{6+} $3d_{3/2}$ (BE ≅ 235.8 eV) lines of Mo oxide species. However, the Mo 3*d* X-ray photoelectron spectra are in no way able to provide information on the coordination geometry of Mo^{6+}. The sulfidation converts most of Mo^{6+} into Mo^{4+}, and probably leads to the formation of MoS_2 (Fig. 4B). However, the sulfidation of zeolite-supported Ni–Mo catalysts is not as complete as for Al_2O_3-supported catalysts. The Mo 3*d* X-ray photoelectron spectra of the sulfided Ni–Mo catalysts were decomposed into three sets of doublets, corresponding to Mo^{6+}, Mo^{5+}, and Mo^{4+} species in order of decreasing binding energy and a broad peak at about 226.3 eV assigned to the S 2*s* line (24). The Mo^{6+} species may be MoO_3 or some other oxide phases that are not completely sulfided, the Mo^{5+} species may be a Mo oxysulfide species, and the Mo^{4+} species are MoS_2 and the Ni–Mo–S phase.

Figure 5 shows the Ni 2*p* X-ray photoelectron spectra of calcined and sulfided Ni–Mo catalysts supported on zeolites. The two main peaks in the X-ray photoelectron spectra of the calcined samples are assigned to the spin–orbit split Ni $2p_{3/2}$ (BE ≅ 856.3 eV) and Ni $2p_{1/2}$ (BE ≅ 873.8 eV) lines and the two broad peaks to the envelopes of the corresponding satellite lines. The Ni 2*p* X-ray photoelectron spectra suggest that the Ni species in the calcined catalysts can be assigned to Ni^{2+} in interaction with zeolites and/or with molybdenia, as expected. The Ni 2*p* X-ray photoelectron spectra of the sulfided catalysts are more complex, decomposing into two sets of Gaussian components: one for the Ni oxide species, as seen in the calcined catalysts, and the other for the Ni sulfide species. The Ni sulfide species are assumed to be Ni_3S_2 at the sulfiding conditions and the so-called Ni–Mo–S phase responsible for the active catalysis.

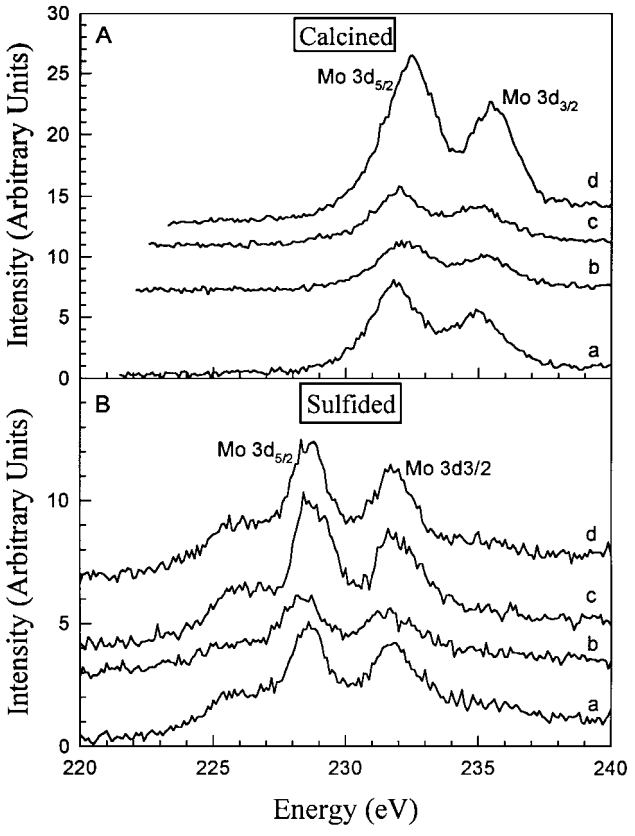

FIG. 4. Mo 3*d* XPS spectra of calcined (A) and sulfided (B) Ni–Mo catalysts supported on zeolites. (a) Ni–Mo/NaY zeolite. (b) Ni–Mo/USY zeolite. (c) Ni–Mo/H-mordenite. (d) Ni–Mo/ZSM-5.

The atomic concentrations of Ni and Mo species on the surface of calcined and sulfided Ni–Mo catalysts supported on zeolites were calculated (24). The Ni/Si and Mo/Si atomic ratios on the surfaces of catalysts and in the corresponding bulks are compared in Table 4. The sulfidation degrees of Ni and Mo species are calculated based on the atomic concentration ratios of the corresponding sulfide species over the oxide species and are included in Table 4. The Ni/Si and Mo/Si atomic ratios in the bulk catalysts are calculated

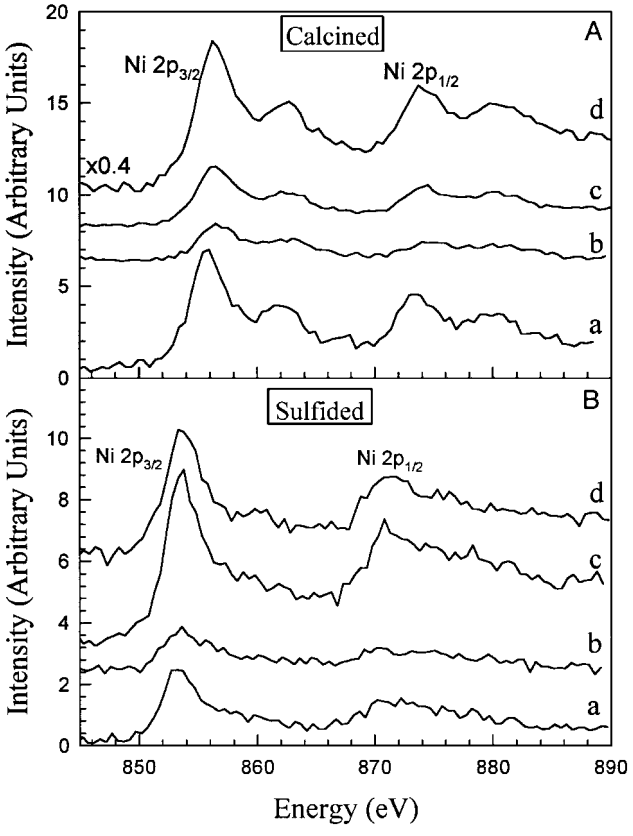

FIG. 5. Ni 2*p* XPS spectra of calcined (A) and sulfided (B) Ni–Mo catalysts supported on zeolites. (a) Ni–Mo/NaY zeolite. (b) Ni–Mo/USY zeolite. (c) Ni–Mo/H-mordenite. (d) Ni–Mo/ZSM-5.

based on the chemical composition of zeolite-supported Ni–Mo catalysts, in which Ni and Mo were analyzed by irradiated neutron activation analysis, and Si, Al, and Na by inductively coupled plasma emission spectroscopy. The Ni/Si and Mo/Si atomic ratios on the surface of calcined Ni–Mo/NaY, Ni–Mo/mordenite, and Ni–Mo/ZSM-5 are higher than those in the corresponding bulk materials, indicating that Ni and Mo are enriched on the surface of the catalysts. However, the unusually high Ni/Si and Mo/Si ratios on the surface of Ni–Mo/ZSm-5 were unexpected. After sulfidation, the Ni/Si and Mo/Si atomic ratios on the surface of these catalysts indicate that the Ni and Mo species tend to be redistributed, but the Ni and Mo species are still enriched on the surface. The most significant characteristic is that Ni/Si and Mo/Si atomic ratios on the surface of calcined Ni–Mo/USY zeolite are very close to those in the bulk material, indicating that both Ni and Mo are relatively homogeneously distributed in the Ni–Mi/USY catalysts at a macroscopic level. After sulfidation, the Ni/Si and Mo/Si ratios are still small on the surface of sulfided Ni–Mo/USY catalyst. The sulfidation degree of both Ni and Mo species in the Ni–Mo/USY is slightly smaller than for the other zeolite supported Ni–Mo catalysts. These results imply that Ni and Mo may be incorporated into the crystal structure of USY zeolite.

Structure and Chemical State of Ni and Mo Species in Bulk Catalysts

The XRD patterns of zeolites and their corresponding calcined Ni–Mo catalysts are almost identical. There is no XRD evidence for the presence of crystalline Ni and Mo oxide phases in the Ni–Mo catalysts. This suggests that particles of Ni and Mo oxide phases, if present, are on the nanometer scale. Thus, conventional powder XRD provides little information on the identity of the Ni–Mo oxide species in these catalysts.

Figure 6 shows the diffuse reflectance spectra of Ni–Mo catalysts supported on NaY zeolite, USY zeolite, mordenite, and ZSM-5 in the range 200–2500 nm. The DRS features in the range 500–1800 nm are shown in the inset. There are strong UV absorption peaks at about 300 nm, which are attributed to Mo species. The features in the range 500–1300 nm may be related to Ni species. By comparison with the background diffuse reflectance spectrum of the sample cell, the weak peak at 1385 nm is attributed to the cell window. Peaks at 1417 nm (7042 cm^{-1}), 1916 nm (5208 cm^{-1}), and 2215 nm (4515 cm^{-1}) are attributed to the first overtone of the fundamental O–H stretching vibration, the combination stretching and bending mode of H_2O molecules, and the combination stretching and bending of structural X–OH groups (X = Al or Si), respectively (29), although the peak at 2215 nm may have a

TABLE 4

Atomic Concentrations of Ni and Mo on Calcined and Sulfided Catalysts Supported on Zeolites

	Oxide		Sulfide		Bulk		Sulfidation[a]	
Catalyst	Ni/Si	Mo/Si	Ni/Si	Mo/Si	Ni/Si	Mo/Si	Ni (%)	Mo (%)
Ni–Mo/NaY	0.0780	0.0824	0.0255	0.0395	0.0166	0.0348	70.5	56.3
Ni–Mo/USY	0.0214	0.0384	0.0120	0.0218	0.0236	0.0514	62.8	54.4
Ni–Mo/mordenite	0.0333	0.0435	0.0555	0.0468	0.0203	0.0183	68.3	60.1
Ni–Mo/ZSM-5	0.1794	0.1778	0.0365	0.0388	0.0133	0.0270	70.1	68.8

[a] Ni sulfidation $= I_{\text{Ni sulfides}}/(I_{\text{Ni sulfides}} + I_{\text{Ni oxides}})$. Mo sulfidation $= I_{\text{Mo sulfides}}/(I_{\text{Mo sulfides}} + I_{\text{Mo oxosulfides}} + I_{\text{Mo oxides}})$.

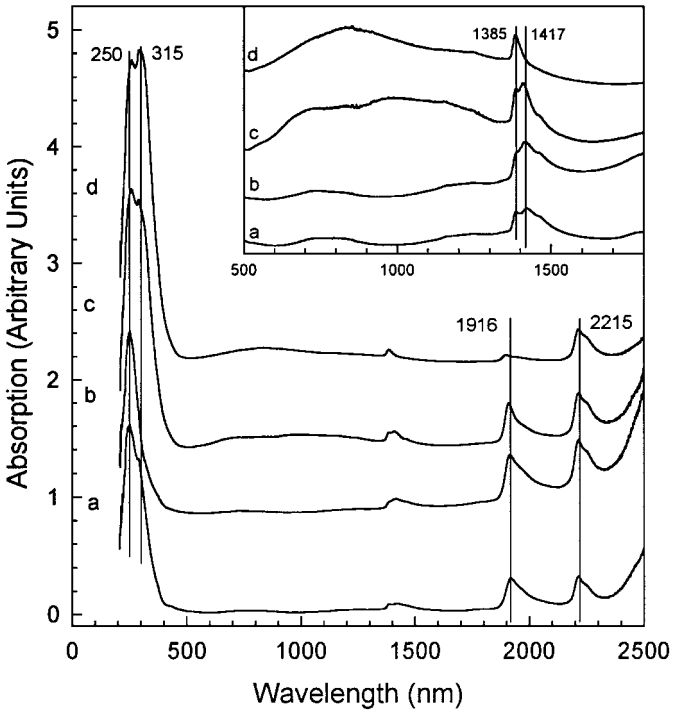

FIG. 6. Diffuse reflectance spectra of calcined Ni–Mo catalysts supported on zeolite in the range 200–2500 nm. (a) Ni–Mo/NaY zeolite. (b) Ni–Mo/USY zeolite. (c) Ni–Mo/H-mordenite. (d) Ni–Mo/ZSM-5.

contribution from the sample cell window. The relative intensities of the two peaks at 1919 and 2215 nm are smaller in Ni–Mo/NaY than in Ni–Mo/USY, and become very small in Ni–Mo/ZSM-5, in agreement with the above assignments.

There are two broad absorption bands between 500 and 1200 nm: one is at about 710 nm, and the other at about 1120 nm. In addition, another absorption band at about 400 nm has been observed for our Ni-loading zeolite sample (unpublished data), which may overlap with the strong absorption bands between 200 and 400 nm in the diffuse reflectance spectrum of zeolite-supported Ni–Mo catalysts. By comparison, the crystal field spectrum of crystalline $CaNiSi_2O_6$ shows three main absorption bands corresponding to the three allowed transitions characteristic of six-coordinated Ni^{2+} ($^{[6]}Ni^{2+}$): $^3A_{2g}(^3F) \rightarrow {}^3T_{2g}(^3F)$ (crystal field transition) at 8200 cm^{-1} (1220 nm), $^3A_{2g}(^3F) \rightarrow {}^3T_{1g}(^3F)$ at 13,170 cm^{-1} (758 nm), and $^3A_{2g}(^3F) \rightarrow {}^3T_{2g}(^3P)$ at 24,450 cm^{-1} (409 nm) (30). Thus, the peaks at 400, 710, and 1120 nm are essentially characteristic of six-coordinated Ni^{2+}. These results are in good agreement with Rossman *et al.* (31) and White *et al.* (32), but different from the diffuse reflectance spectra of Lepetit and Che (33) and Schoonheydt *et al.* (34). Lepetit and Che (33) interpreted the absorption bands at 1661, 997, 616, 494, and 467 nm in the diffuse reflectance spectrum of Ni-exchanged faujasite-type zeolites as to Ni^{2+} cations in distorted tetrahedral (T_d) $S_{I'}$ and/or S_{II} sites, and the absorption bands in 1600, 903 and 270 nm to Ni^{2+} cations in trigonal (D_{3h}) coordination in $S_{I'}$ sites. Schoonheydt *et al.* (34) suggested that Ni^{2+} in zeolites X and Y is present in octahedral coordination in the hexagonal prisms (S_I), trigonal coordination in the sodalite cage ($S_{I'}$), and tetrahedral coordination in the sodalite cage ($S_{I'}$).

Figure 7 shows the UV–vis region of the diffuse reflectance spectra of Ni–Mo/NaY, Ni–Mo/USY, Ni–Mo/mordenite, and Ni–Mo/ZSM-5. The spectra were deconvoluted into Gaussian components (peaks A, B, and C) by fitting. Peaks A, B, and C tend to increase in amplitude from Ni–Mo/USY, through Ni–Mo/NaY and Ni–Mo/mordenite, to Ni–Mo/ZSM-5. These peaks are assigned to Mo–O charge transfer of Mo^{6+} species. Peak A is further attributed to tetrahedral-coordinated Mo^{6+} species, and peaks B and C to octahedral-coordinated Mo^{6+} species (35, 36). Peak C is characteristic of MoO_3. Thus,

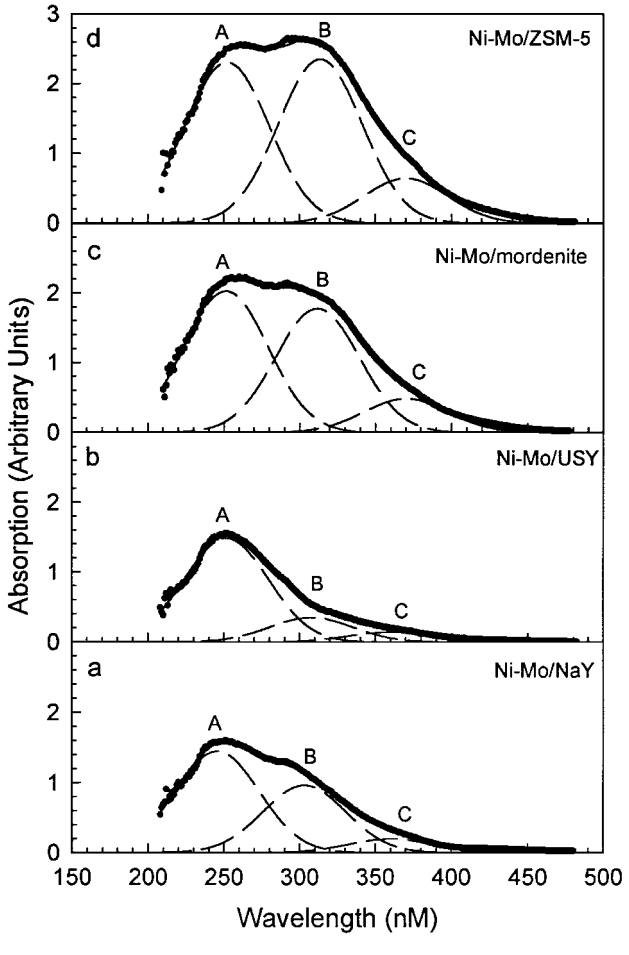

FIG. 7. UV–vis diffuse reflectance spectra of calcined Ni–Mo catalysts supported on zeolites in the range 150–500 nm, which were decomposed by fitting. (a) Ni–Mo/NaY zeolite. (b) Ni–Mo/USY zeolite. (c) Ni–Mo/H-mordenite. (d) Ni–Mo/ZSM-5.

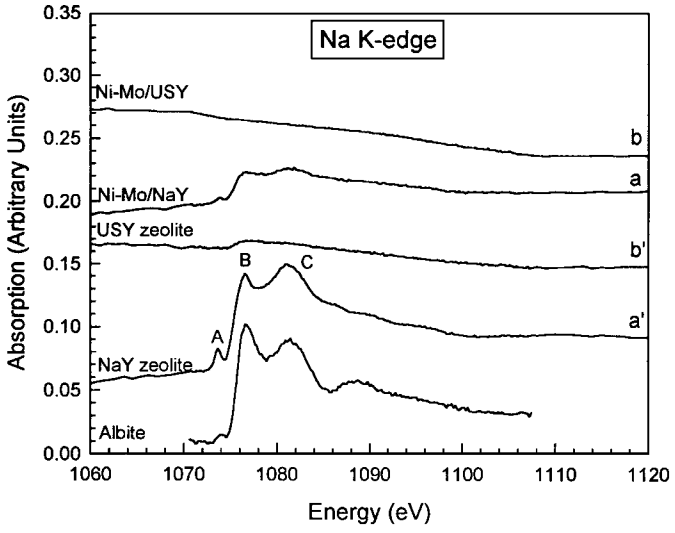

FIG. 8. Na *K*-edge XANES spectra of NaY zeolite (a′), USY zeolite (b′), Ni–Mo/NaY (a), and Ni–Mo/USY (b), in comparison with Na *K*-edge spectrum of albite.

the dominant amount (>80%) of Mo^{6+} in Ni–Mo/USY is four-coordinated ($^{[4]}Mo^{6+}$) with oxygen. From Ni–Mo/USY, through Ni–Mo/NAY and Ni–Mo/mordenite, to Ni–Mo/ZSM-5, the proportion of six-coordinated Mo^{6+} ($^{[6]}Mo^{6+}$) including MoO_3 dramatically increases, and the ratio of $^{[4]}Mo^{6+}/^{[6]}Mo^{6+}$ significantly decreases in this order.

Structural Changes of Na and Al in Zeolites during Catalyst Preparation

Figure 8 shows Na *K*-edge XANES spectra of NaY zeolite, USY zeolite, Ni–Mo/NaY, and Ni–Mo/USY, in comparison with Na *K*-edge spectrum of albite. The interpretation of such XANES spectra is very controversial. The classic explanation is based on molecular orbital theory, which interpreted the *K*-edge peak to the electronic transition from 1*s* to empty bound *p*-like states. Another more popular interpretation over the last decade is multiple scattering (MS) theory. It is impossible to interpret the Na *K*-edge XANES spectra without quantitative theoretical calculations. However, tentatively we assign peak B to the edge peak, attributed to the electronic transition of 1*s* electrons to empty 3*p*-like states; peak A to pre-edge, attributed to the transition of 1*s* electrons to empty 3*s*-like states. The Na *K*-edge spectrum of NaY zeolite is very similar to that of albite, indicating that Na is six-coordinated with oxygen in NaY zeolite, in agreement with X-ray crystal structure data. However, the pre-edge peak A is more prominent than observed for albite and many other minerals, indicating that the coordination site of Na is more distorted in NaY zeolite. After dealumination, most Na atoms were eliminated from NaY zeolite (see Table 1), so that the Na *K*-edge spectrum of USY zeolite is weak, but similar to that of NaY. The Na *K*-edge spectrum of Ni–Mo/NaY is similar to that of NaY zeolite, but the intensity of the peaks decreases, indicating that about 70% of Na atoms in NaY zeolite were ion-exchanged by Ni and/or Mo during catalyst preparation. In Ni–Mo/USY zeolite, the Na content is so low that no signals in the Na *K*-edge spectrum were observed.

Figure 9 shows Al *K*-edge XANES spectra of NaY zeolite, USY zeolite, Ni–Mo/NaY, and Ni–Mo/USY, in comparison with the Al *K*-edge spectrum of α-Al_2O_3. Again, the prominent peak at about 1565.7 eV in the Al *K*-edge spectrum of NaY zeolite is assigned to the transition of 1*s* electrons to empty 3*p*-like states of Al in tetrahedral coordination. Using NaY zeolite as a model, the Al *K*-edge peak amplitudes of USY zeolite, Ni–Mo/NaY, and Ni–Mo/USY were equated to that of NaY zeolite, and difference spectra were determined. Although the difference spectra are noisy, they indicate the presence of extra-framework Al ($^{[6]}$Al) in Ni–Mo/NaY and Ni–Mo/USY catalysts, but the $^{[6]}$Al may be present at a marginal level (<3%) in the

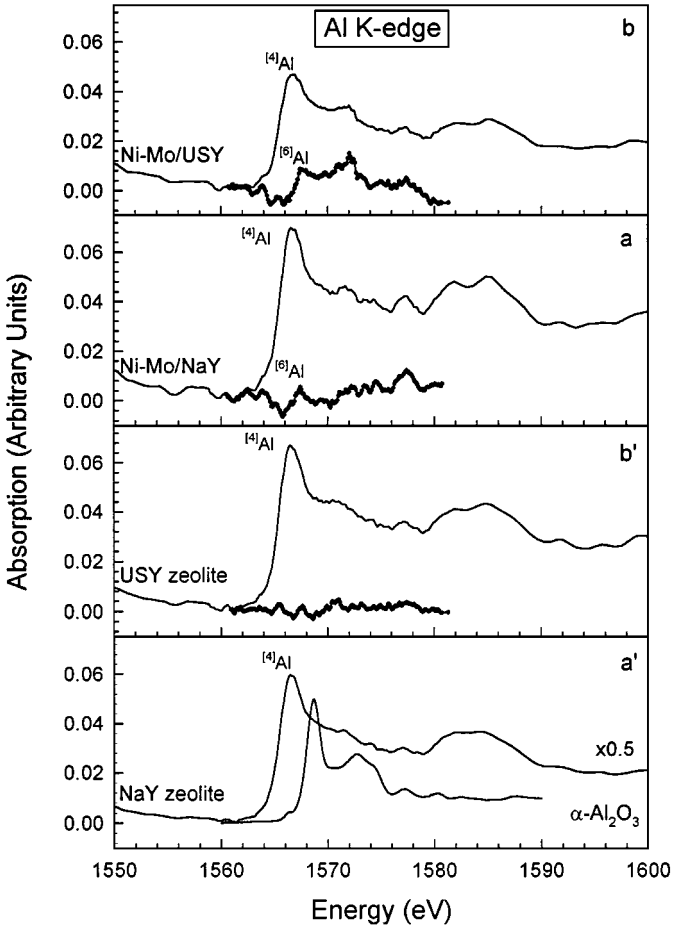

FIG. 9. Al *K*-edge XANES spectra of NaY zeolite (a′), USY zeolite (b′), Ni–Mo/NaY (a), and Ni–Mo/USY (b), in comparison with Al *K*-edge spectrum of α-Al_2O_3. The filled dot lines are the difference spectra between these samples and NaY zeolite by aligning the amplitude of $^{[4]}$Al peak in NaY zeolite spectrum to that of $^{[4]}$Al peak in the other samples.

USY zeolite. It is estimated that the amount of $^{[6]}$Al in Ni–Mo/NaY and Ni–Mo/USY is about 8 and 18% of the total Al, respectively, based on the relative intensity (amplitude) of the edge peaks for $^{[6]}$Al and $^{[4]}$Al. Thus, during dealumination, Al was eliminated from the framework by steaming, but after washing many times, the resulting USY zeolite contains very little extra-framework Al species. However, during the ion exchange of Ni–Mo solution with NaY and USY zeolites and subsequent calcination at 550°C to prepare zeolite-supported Ni–Mo catalysts, dealumination phenomena have been observed.

DISCUSSION

Acidity versus Activity

The acid structure of zeolite Y is very complex and controversial (37–42). The detailed nature of the acid structure is not addressed in the present work. However, by comparing the NH_3 TPD spectra of NaY and USY zeolites and their supported Ni–Mo catalysts, a very prominent high-temperature peak at about 430°C in the NH_3 TPD spectrum of USY zeolite and its supported catalyst can be interpreted as due to protonic Brønsted acid sites. These Brønsted acid sites in USY zeolite contribute to the difference in HC activities between NaY and USY zeolites, which is most evident in the HC of diphenylmethan (Fig. 1D).

There are hydroxyls interacting with extra-framework aluminum in dealuminated zeolites that also contribute to the Brønsted acidity (41, 43). However, the Al *K*-edge XANES spectra (Fig. 9) show that the amount of extra-framework Al in the USY zeolite is very low (<3%), close to the detection limit of the Al *K*-edge XANES technique. Thus, the high-temperature peak in the NH_3 TPD spectrum of USY zeolite and its Brønsted acidity are dominantly related to hydroxyls in interaction with framework Al.

Al *K*-edge XANES spectra of Ni–Mo/NaY and Ni–Mo/USY showed the presence of some extra-framework Al, which is produced during the ion exchange and/or subsequent calcination of zeolite-supported catalysts. The NH_3 TPD spectra of Ni–Mo/NaY and Ni–Mo/USY are almost identical to those of NaY and USY zeolite, respectively, confirming that the extra-framework Al in zeolite-supported Ni–Mo catalysts contributes little to their acid structures. The HDS activity of DBT and the HC activities of decalin, tetralin, and DPM over Ni–Mo/USY are much higher than those for USY zeolite and Ni–Mo/NaY, indicating that the Brønsted acidity in Ni–Mo/USY partially contributes to the high catalytic activities of this catalyst, which is also related to the loading Ni and Mo phases.

Structure of Ni and Mo Species versus Activity

There are both four- and six-coordinated Mo oxide species in the zeolite-supported Ni–Mo catalysts. The six-coordinated Mo oxide species is most likely to be MoO_3 that is present on the surface of zeolite particles or the mesopores of USY zeolite. In the Ni–Mo/USY zeolite, the dominant amount of Mo species is four-coordinated, and this Mo species may be present in the sodalite cage and/or supercage of the USY zeolite, although the possibility of its presence in the mesopores of USY zeolite is not excluded. Ni is dominantly six-coordinated in all zeolite-supported Ni–Mo catalysts, but the exact locations of Ni in these catalysts are unknown. It has been proven that Na may be present in hexagonal prisms (S_I), sodalite cage ($S_{I'}$, $S_{II'}$), and/or supercage (S_{II}, S_{III}) of NaY zeolite (44). In Ni–Mo/NaY zeolite catalyst, the large amount (~70%) of Na in NaY zeolite is exchanged by Ni and/or Mo. Thus, it is deduced that Na may preferentially locate in sodalite cage and/or supercage. Whether a nanometer-size Ni–Mo oxide (e.g., $NiMoO_4$) may form in the sodalite cage and/or supercage of USY zeolite is unknown. However, it appears that the six-coordinated Ni and four-coordinated Mo located in the sodalite cage and/or supercage of USY zeolite make a major contribution to the high catalytic HC and HDS activities of these model reactions. The Ni and Mo species may interact with the Brønsted acid sites also in the sodalite cage and/or supercage of USY zeolite, so that the loading of Ni and Mo species and the Brønsted acidity may make a synergistic contribution to the high catalytic HC and HDS activities of USY-supported Ni–Mo catalyst.

CONCLUSIONS

USY-supported Ni–Mo sulfide catalyst has an unusually high catalytic activity for hydrodesulfurization of dibenzothiophene and hydrocracking of decalin, tetralin, and diphenylmethan, compared with the other zeolites and their supported Ni–Mo catalysts, and it also has much higher HDS and HC activities than Al_2O_3-supported catalyst. NH_3 TPD indicated the presence of a very strong Brønsted acid site in the USY zeolite, which is associated with the framework aluminum. Although some extra-framework aluminum is produced during the ion exchange of Ni–Mo solution with zeolite Y and/or the subsequent calcination at 550°C, the strong Brønsted acid site is apparently not related to the extra-framework aluminum. There is also no evidence showing that the extra-framework aluminum has made a significant contribution to the catalytic activity of the tested reactions. The surface concentrations of Ni and Mo are high on the surface of Ni–Mo/NaY, Ni–Mo/mordenite, and Ni–Mo/ZSM-5, implying that Ni and Mo species may form aggregations on the surface of the zeolite particles. Alternatively, Ni and Mo may enter the lattice structure of USY zeolite or may be present in the mesopores of USY zeolite. Ni is six-coordinated and Mo is dominantly four-coordinated in the Ni–Mo/USY. Although the exact locations of Ni and Mo species are unknown, it

is deduced that they may be present in the sodalite cage and/or supercage. Thus, both the strong Brønsted acid sites and the Ni–Mo sulfide phases in the sodalite cage and/or supercage of USY zeolite may contribute to the high HDS and HC activities of USY zeolite-supported Ni–Mo sulifide catalyst.

ACKNOWLEDGMENTS

D.L. appreciates the support from the STA fellowship from Science and Technology Agency (STA) of Japan. We thank K. Masuda, Catalysts & Chemical Industry Ltd., Japan, for his technical assistance; the staff at UVSOR, Institute of Molecular Sciences, and T. Murata, Kyoto University of Education, for their technical assistance with Na and Al *K*-edge XANES measurements; and B. Carey, Los Alamos National Laboratory, for his thorough review of this manuscript.

REFERENCES

1. Topsoe, H., Clausen, B. S., and Massoth, F. E., "Hydrotreating Catalysis: Science and Technology," p. 310. Spinger-Verlag, Berlin, 1996.
2. Maxwell, I. E., *Catal. Today* **1**, 385 (1987).
3. Vasudevan, P. T., and Fierro, J. L. G., *Catal. Rev. Sci. Eng.* **38**, 161 (1996).
4. Vazquez, M. I., Escardino, A., Aucejo, A., and Corma, A., *Can. J. Chem. Eng.* **64**, 272 (1986).
5. Vazquez, M. I., Escardino, A., and Aucejo, A., *Ind. Eng. Chem. Res.* **27**, 2039 (1988).
6. Baudon, A., Lemberton, J. L., Guisnet, M., Marchal, N., and Mignard, S., *Catal. Lett.* **36**, 245 (1996).
7. Vazquez, M. I., Escardino, A., and Corma, A., *Ind. Eng. Chem. Res.* **26**, 1495 (1987).
8. Welters, W. J. J., van der Waerden, O. H., de Beer, V. H. J., and van Santen, R. A., *Ind. Eng. Chem. Res.* **34**, 1166 (1995).
9. Egia, B., Cambra, J. F., Guemez, B., Arias, P. L., Pawelec, B., and Fierro, J. L. G., *in* "Hydrotreatment and Hydrocracking of Oil Fractions" (G. F. Froment, B. Delmon, and P. Grange, Eds.), p. 567. Elsevier Science, Amsterdam, 1997.
10. Cid, R., Villasenor, J., Orellana, F., Fierro, J. L. G., and Lopez Agudo, A., *Appl. Catal.* **18**, 357 (1985).
11. Cid, R., Orellana, F., and Lopez Agudo, A., *Appl. Catal.* **32**, 327 (1987).
12. Corma, A., Vazquez, M. I., Bianconi, A., Clozza, A., Garcia, J., Pallota, O., and Cruz, G. M., *Zeolites* **8**, 464 (1988).
13. Spojakina, A. A., and Kostova, N., *Collect. Czech. Chem. Commun.* **57**, 2509 (1992).
14. Okamoto, Y., and Katsuyama, H., *Stud. Surf. Sci. Catal.* **101**, 503 (1996).
15. Okamoto, Y., and Katsuyama, H., *AIChE J.* **43**, 2809 (1997).
16. Davidova, N., Kovacheva, P., and Shopov, D., *Zeolites* **5**, 659 (1985).
17. Kovacheva, P., Davidova, N., and Novakova, J., *Zeolites* **11**, 54 (1991).
18. Tatsumi, T., Taniguchi, M., Ishige, H., Ishii, Y., Murata, T., and Hidai, M., *Appl. Catal.* **121/122**, 500 (1997).
19. Cid, R., Gil Llambias, F. J., Gonzalez, M., and Lopez Agudo, A., *Catal. Lett.* **24**, 147 (1994).
20. Leglise, J., Janin, A., Lavalley, J. C., and Cornet, D., *J. Catal.* **114**, 388 (1988).
21. Leglise, J., el Qotbi, M., Goupil, J. M., and Cornet, D., *Catal. Lett.* **10**, 103 (1991).
22. Leglise, J., Manoli, J. M., Potvin, C., Djega-Mariadassou, G., and Cornet, D., *J. Catal.* **152**, 275 (1995).
23. Welters, W. J. J., Vorbeck, G., Zandbergen, H. W., de Haan, J. W., de Beer, V. H. J., and van Santen, R. A., *J. Catal.* **150**, 155 (1994).
24. Li, Dien, Sato, T., Imamura, M., Shimada, H., and Nishijima, A., *J. Catal.* **170**, 357 (1997).
25. Kerkhof, F. P. J. M., and Moulijn, J. A., *J. Phys. Chem.* **83**, 1612 (1979).
26. Li, Dien, Sato, T., Imamura, M., Shimada, H., and Nishijima, A., *Appl. Catal. B* **16**, 255 (1998).
27. Haag, W. O., Lago, R. M., and Weisz, P. B., *Nature* **309**, 589 (1982).
28. Xu, Y. D., Shu, Y. Y., Liu, S. T., Huang, J. S., and Guo, X. X., *Catal. Lett.* **35**, 233 (1995).
29. Stopler, E., *Contrib. Mineral. Petrol.* **81**, 1 (1982).
30. Galoisy, L., and Calas, G., *Am. Mineral.* **76**, 1777 (1991).
31. Rossman, G. R., Shannon, R. D., and Waring, R. K., *J. Solid State Chem.* **39**, 277 (1981).
32. White, W. B., McCarthy, G. J., and Scheetz, B. E., *Am. Mineral.* **56**, 72 (1971).
33. Lepetit, C., and Che, M., *J. Phys. Chem.* **100**, 3137 (1996).
34. Schoonheydt, R. A., Roodhooft, D., and Leeman, H., *Zeolites* **7**, 412 (1987).
35. Jezlorowski, H., and Knözinger, H., *J. Phys. Chem.* **83**, 1166 (1979).
36. Williams, C. C., Ekerdt, J. G., Jehng, J. M., Hardcastle, F. D., and Wachs, I. E., *J. Phys. Chem.* **95**, 8791 (1991).
37. Karge, H. G., Dondur, V., and Weitkamp, J., *J. Phys. Chem.* **95**, 283 (1991).
38. Miessner, H., Kosslick, H., Lohse, U., Parlitz, B., and Yuan, V. A., *J. Phys. Chem.* **97**, 9741 (1993).
39. Biaglow, A. I., Parrillo, D. J., Kokotailo, G. T., and Gorte, R. J., *J. Catal.* **148**, 213 (1994).
40. Kiricsi, I., Flego, C., Pazzuconi, G., Parker, W. O. Jr., Millini, R., Perego, C., and Bellussi, G., *J. Phys. Chem.* **98**, 4627 (1994).
41. Datka, J., Sulikowski, B., and Gil, B., *J. Phys. Chem.* **100**, 11242 (1996).
42. Kuehne, M. A., Babitz, S. M., Kung, H. H., and Miller, J. T., *Appl. Catal. A* **66**, 293 (1998).
43. Makarova, M. A., and Dwyer, J., *J. Phys. Chem.* **97**, 6337 (1997).
44. Verhulst, H. A. M., Welters, W. J. J., Vorbeck, G., van de Ven, L. J. M., de Beer, V. H. J., van Santen, R. A., and de Haan, J. W., *J. Phys. Chem.* **98**, 7056 (1994).